UC Davis

UC Davis Previously Published Works

Title

Polystyrene-modified carbon nanotubes: Promising carriers in targeted drug delivery.

Permalink

https://escholarship.org/uc/item/307750x7

Journal

Authors

Gul, Gulsah

Ileri-Ercan, Nazar

Faller, Roland

Publication Date

DOI

Peer reviewed

Article

Polystyrene-modified carbon nanotubes: Promising carriers in targeted drug delivery

Gulsah Gul,[1,2] Roland Faller,[2] and Nazar Ileri-Ercan[1,*]
[1]Department of Chemical Engineering, Bogazici University, Bebek, Istanbul, Turkey and [2]Department of Chemical Engineering, University of California, Davis, Davis, California

ABSTRACT   To design drug-delivery agents for therapeutic and diagnostic applications, understanding the mechanisms by which covalently functionalized carbon nanotubes penetrate and interact with cell membranes is of great importance. Here, we report all-atom molecular dynamics results from polystyrene and carboxyl-terminated polystyrene-modified carbon nanotubes and show their translocation behavior across a model lipid bilayer together with their potential to deliver a molecule of the drug ibuprofen into the cell. Our results indicate that functionalized carbon nanotubes are internalized by the membrane in hundreds of nanoseconds and that drug loading increases the internalization speed further. Both loaded and unloaded tubes cross the closest leaflet of the bilayer by nonendocytic pathways, and for the times studied, the drug molecule remains trapped inside the pristine tube while remaining attached at the end of polystyrene-modified tube. On the other hand, carboxyl-terminated polystyrene functionalization allows the drug to be completely released into the lower leaflet of the bilayer without imposing damage to the membrane. This study shows that polystyrene functionalization is a promising alternative and facilitates drug delivery as a benchmark case.

SIGNIFICANCE   We report all-atom molecular dynamics results from polystyrene and carboxyl-terminated polystyrene-modified carbon nanotubes and show their translocation behavior across a model lipid bilayer together with their potential to deliver a drug molecule into the cell. Our results indicate that no damage occurs in the membrane integrity during the penetration of carbon nanotubes, drug-loaded and nonloaded carbon tubes cross the bilayer by nonendocytic pathways, and polystyrene functionalization of carbon nanotubes facilitates the delivery of ibuprofen.

INTRODUCTION

Having attracted great scientific interest due to their specific structures, superior thermal, and electrical features (1–3), carbon nanotubes (CNTs) can easily penetrate mammalian cells and effectively transport molecular drugs to the targeted cytoplasm or nucleus in vitro (4–6). However, CNTs suffer from nonuniform dispersion in polymer matrices, insolubility in several aqueous and organic solvents, and potential toxic responses when used as antitumor drug carriers in clinical applications (7). To overcome these limitations, CNTs have been functionalized with various functional groups, including polymers (8–10). Increased dispersion and solubility behavior of nanotubes due to polymer modification (11) has been reported to improve performance and reduce toxicity (12,13).

In experimental studies, short (<5 μm) and highly dispersed CNTs were reported to have low toxicity in mice (14,15), whereas longer CNTs can trigger mesothelioma (14). PEG-functionalized CNTs demonstrated low toxicity, long blood circulation time (up to ~22 h), and more effective clearance in mice on the lab (16,17) and pilot scales (18). Moreover, single-walled CNTs (SWCNTs) modified with hexamethylenediamine and poly(diallyldimethylammonium)chloride show noncovalent binding of negatively charged small interfering RNA and exhibit an efficient intracellular delivery with few cytotoxic effects on rat heart cells up to a concentration level of 10 mg/L (19). Polymer modification of CNTs was also examined computationally in atomistic (20) and CG detail (21), where the chain size and grafting density were found to influence the conformation of the conjugated PEG chains consistent with the experimentally proposed conformation of PEGs in the mushroom-brush transition regime (21).
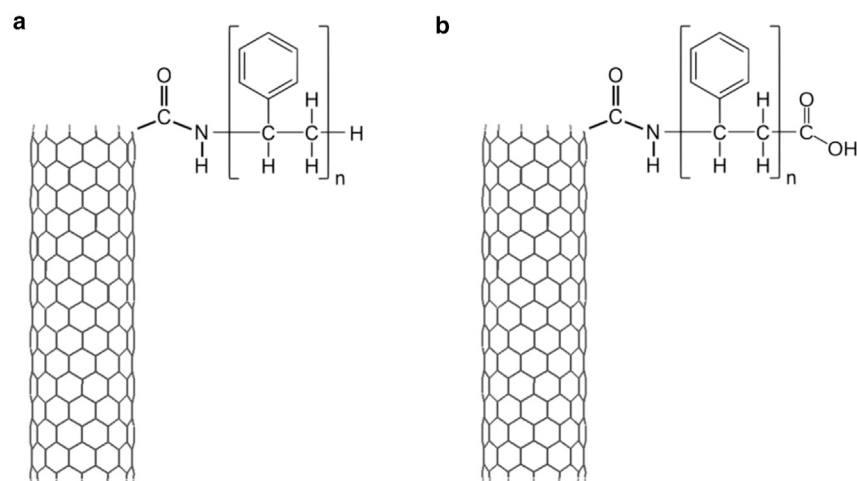
a   **b**

FIGURE 1 Functionalization of CNTs with PS (*a*) and PSCOOH (*b*) via amidation reaction. Here, *n* shows the number of monomers of the polymer, which is taken as 29 in this study.

Although studies carried out to date are mainly focused on PEG modification, it has been previously demonstrated that polystyrene, specifically with carboxyl groups, can be a safe alternative compared with a wide range of inorganic and organic nanoparticle (NP) materials (22). Studies involving the polystyrene (PS) functionalization of CNTs, on the other hand, are scarce and have focused on the solubility and dispersion ability to obtain nanocomposite materials with desired properties. For example, a significant increase in tensile modulus and break stress was recorded with the dispersion of CNTs in PS matrices (23,24), and high solubility in organic solvents was obtained (25–27). A linear relation was found between the strength and chain density of the grafted PS (24). On the other hand, PS-modified CNTs as drug-delivery systems have been rarely studied. Tabet et al. studied the cytotoxicity of PS-coated multiwalled CNTs in vitro in murine macrophages and in vivo in mice lungs for a 6 month period and reported that PS coating decreases oxidative stress and inflammation in both and prevents pulmonary toxicity (28). To the best of our knowledge, there is no other experimental or computational study in this context despite their improved performance and potential in drug-delivery systems. To fill this gap in the literature and to shed light on future experimental studies, here we develop all-atom molecular dynamics (MD) models of PS and carboxyl-ended PS (PSCOOH)-functionalized SWCNTs and investigate their translocation behavior across a lipid bilayer. Also, we encapsulate a molecule of poorly water-soluble ibuprofen (IBU) drug in the developed CNT models to mimic the drug-delivery process, which has been investigated in experimental studies to observe the in vitro drug-release profiles of functionalized CNTs (29,30). Our study shows that PS functionalization does not cause toxicity in terms of disruption of membrane integrity and facilitates the delivery of IBU through the PSCOOH-modified CNT.

Simulation parameters

Initial configurations of the SWCNT (31), PS (32), amide, carboxyl, IBU (33), and lipid bilayers (34–36) were generated via CHARMM-GUI software (37), and simulations were performed with GROMACS v.2021.3 (38). Functionalized SWCNTs were formed through visual MD (39) by removing H bonds in the end ring and covalently bonding PS or carboxyl-modified PS with an amide linker as previously described in experimental studies (40–43) (c.f. Fig. 1).

SWCNTs were ∼1 nm in diameter and ∼3 nm in length with the chirality of (12,0) to represent the zig-zag configuration of metallic tubes. The simulated systems consisted of 180 POPC lipids and 14,951 water molecules and included 0.15 M NaCl salt to reflect the biological cell environment. The periodic simulation box was 7.7 nm in the *x* and *y* directions and 12.0 nm in the *z* direction. The CHARMM36 force field (44,45) was used for the lipids (46,47), CGenFF 4.5 (48) was used for the linker, functional groups, and IBU, and a CHARMM-compatible INTERFACE force field (49) was used for the nanotube as well as TIP3P as the water model. The partial charges and bonded parameters were obtained from the CGenFF website (https://cgenff.umaryland.edu/) for the IBU, PS, and PSCOOH functionalization with penalty scores between 0 and 5. The PS chain length was considered 29 monomers (∼3 kDa) in atactic form, consistent with the previous PS grafting studies into nanotubes (50–52). First, NPs were equilibrated in the NPT ensemble for 50 and 100 ns for pristine and functionalized SWCNTs, respectively. Then, the IBU drug was loaded to the center of the NPs and equilibrated for an additional 50 ns. The resultant NP configurations were placed 3 nm above the bilayer center with a 45° angle to the bilayer plane in the absence or presence of IBU (c.f. Fig. 2) since it has been previously suggested that initial configurations of CNTs have no effect on their penetration mechanism (53).
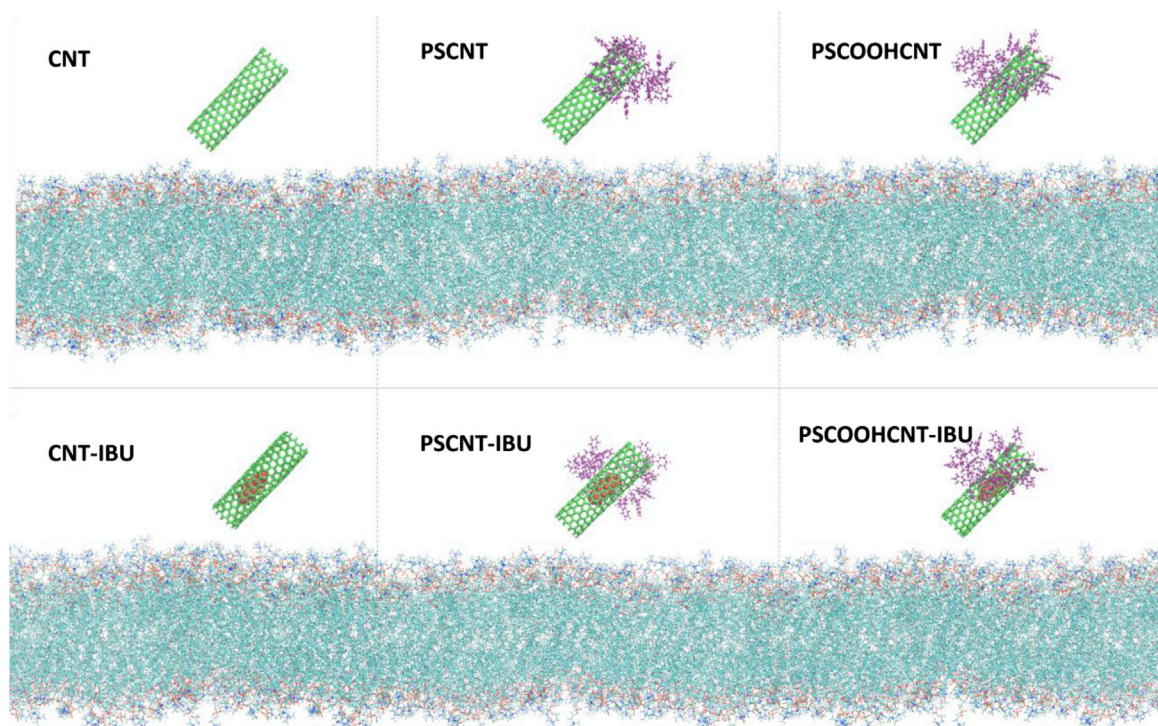
FIGURE 2 Initial configurations of the simulated systems. Here, CNT is in green, PS and PSCOOH are in purple, and IBU is in red. To see this figure in color, go online.

After energy minimization by steepest descent, the systems were equilibrated for 5 ns with 1 fs time step in the NVT ensemble. The temperature was kept at 310 K by velocity rescaling thermostat (54) with a time constant of 1.0 ps. Nonbonded interaction cutoff was applied at 1.2 nm distance, and van der Waals interactions were switched off between 1.0 and 1.2 nm by using the force-switch modifier. The long-range electrostatic interactions were calculated by the particle mesh Ewald algorithm (55) Semi-isotropic pressure coupling was applied at 1 bar by

the Parrinello-Rahman barostat (56) with a coupling constant of 5 ps and a compressibility factor of 4.5×10^{-5} bar^{-1}. Depending on the equilibration time of the systems, simulation times varied between 200 and 710 ns with 2 fs timestep as presented in Table S1. Lastly, 100 or 200 ns of trajectories were used for the analysis depending on the convergence of the measured property.

RESULTS AND DISCUSSION

To elucidate the interaction mechanism of functionalized CNTs with the POPC model bilayer, the structural properties of the lipid bilayer are studied in the presence and absence of IBU. Results are given in Table 1. The computed area-per-lipid and bilayer thickness values of POPC are found to be 0.650 ± 0.012 nm^2 and 3.88 ± 0.06 nm, respectively, in close agreement with experimental data of 0.64–0.68 nm^2 and 3.70–3.91 nm (57,58). In the presence of a NP, the area-per-lipid values slightly decrease except for the no-drug-loaded PS-functionalized CNTs. Yet, the variation in the values is less than 2% for all cases since single nanotube models are used across relatively larger bilayers. The bilayer thickness, on the other hand, slightly increases, with the increase being more pronounced in the presence of the PSCOOH-functionalized nanotubes. This increase, however, is not significant to cause any disruption in the membrane integrity. In other words, pristine and functionalized CNTs permeate into the membrane by passive

TABLE 1 Area per lipid and bilayer thickness values of pure POPC and with pristine/functionalized CNT models, i.e., pristine carbon nanotube (CNT), polystyrene functionalized carbon nanotube (PSCNT), and carboxyl-terminated polystyrene functionalized carbon nanotube (PSCOOHCNT), in the presence and absence of ibuprofen (IBU)

Model	Area per lipid (nm^2)	Bilayer thickness (nm)
POPC	0.650 ± 0.012	3.88 ± 0.06
POPC-CNT	0.641 ± 0.010	3.97 ± 0.05
POPC-PSCNT	0.654 ± 0.011	3.98 ± 0.05
POPC-PSCOOHCNT	0.646 ± 0.012	4.02 ± 0.06
POPC-CNT-IBU	0.638 ± 0.011	3.99 ± 0.05
POPC-PSCNT-IBU	0.649 ± 0.011	4.01 ± 0.06
POPC-PSCOOHCNT-IBU	0.648 ± 0.010	4.02 ± 0.05

The data are obtained from the last 100 and 200 ns of trajectories for systems without and with IBU, respectively. However, in the PSCOOH-CNT-IBU system, the last 100 ns of trajectories are used for the analysis because of the transfer of IBU.
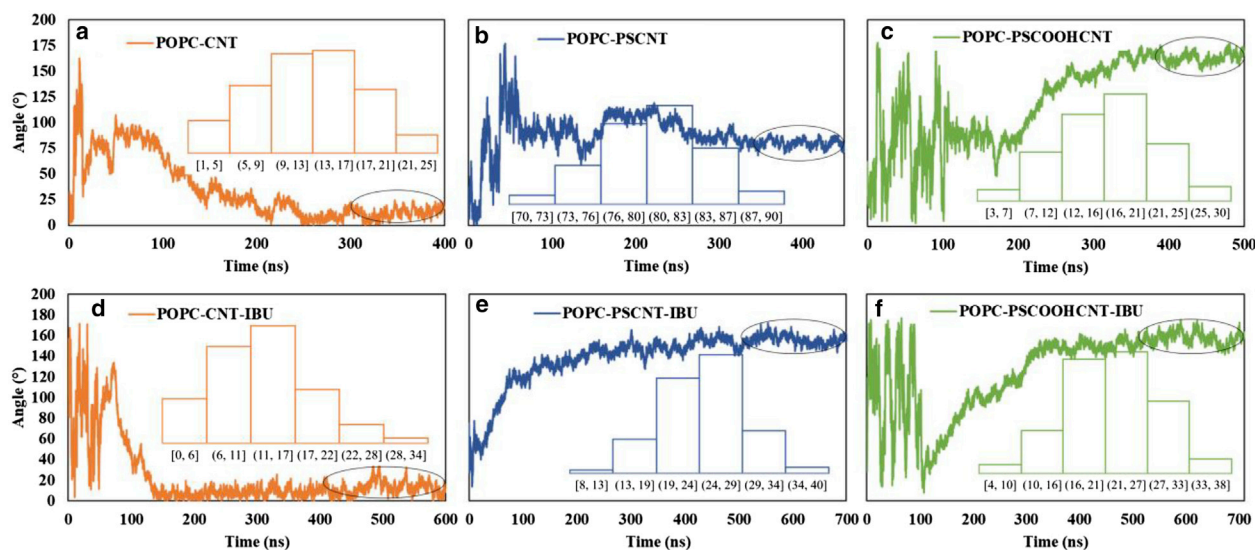
FIGURE 3 The angle distribution between pristine/functionalized CNTs and a lipid bilayer normal in the absence (*top panel*) and presence (*bottom panel*) of IBU. The histograms show acute angle distributions after configurational equilibration of the nanoparticles inside the membrane (last 100 ns for unloaded nanotubes, and last 200 ns for IBU-loaded nanotubes), which is encircled. Angles above 90° demonstrate the rotation of the tubes, hence, values were subtracted from 180° while forming the histograms. To see this figure in color, go online.

diffusion and show no distinct effects on the membrane structure as reported before (53,59,60). In fact, the uptake of SWCNTs strongly depends on the tube's length, and shorter tubes ($\leq 1\ \mu$m) are shown to have a higher tendency to be internalized by the nonendocytic uptake route (59,61).

The change in the angle between the long axis vector of CNT and the bilayer normal during simulation time is given in Fig. 3. The tilt angle for pristine CNTs varies between 0° and 25° with a mean value around 15° in agreement with some experimental findings. A tilt angle between 0° and 15° was observed for short CNTs (D_{in} = 1.5 nm, L = 5–15 nm) in DOPC bilayers by cryogenic TEM analysis, and tube insertion was observed irrespective of the tube length (62). This is also confirmed by Tran et al. through in situ small-angle X-ray scattering measurements; they suggested that the local tilt of the lipids caused by the insertion of CNTs triggers bilayer thinning (63) However, we did not observe this bilayer thinning effect upon CNT insertion in our simulations. More recently, Sullivan et al. proposed a geometrical model by forming a relationship between the variation of tilt angles and apparent CNT height in the atomic

force microscopy images and calculated a broader range of tilt angles (0°–25°) with similar-sized CNTs across equimolar DMPC/DOPC membranes (64) These findings, in general, support the claim that short CNTs (~2 nm in length) orient preferentially parallel to the lipid molecules when embedded within a phospholipid bilayer (65), which is also confirmed by our results. On the other hand, CNTs longer than the bilayer thickness are reported to have larger angles to maximize the interactions between CNT walls and the hydrophobic tail of the lipids (66,67).

Functionalization of CNTs affects the configurational preferences of the tubes and polar functional groups may hinder tilting (67). For example, hydroxyl-modified CNTs have been shown to tend to stand upright in the bilayer center if the length of CNT is less than the bilayer thickness (<4 nm) (60). In this study, the PS-modified CNT prefers to be in a near-horizontal configuration with a tilt angle of ~82° (c.f. Fig. 3 b). The PSCOOH-functionalized nanotube, however, rotates and tilt with an angle less than 30° so that the linker atoms stay close to the headgroups of the lower leaflet (c.f. Fig. 3 c). Furthermore, encapsulating IBU drug
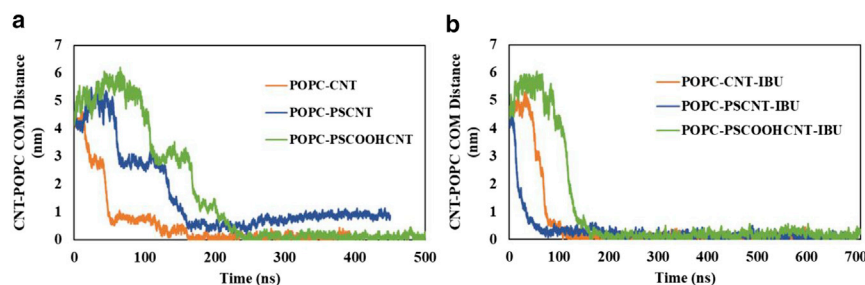

FIGURE 4 The absolute center-of-mass distance of CNTs from the POPC bilayer center for the pristine and functionalized CNTs (*a*) in the absence of IBU and (*b*) in the presence of IBU.
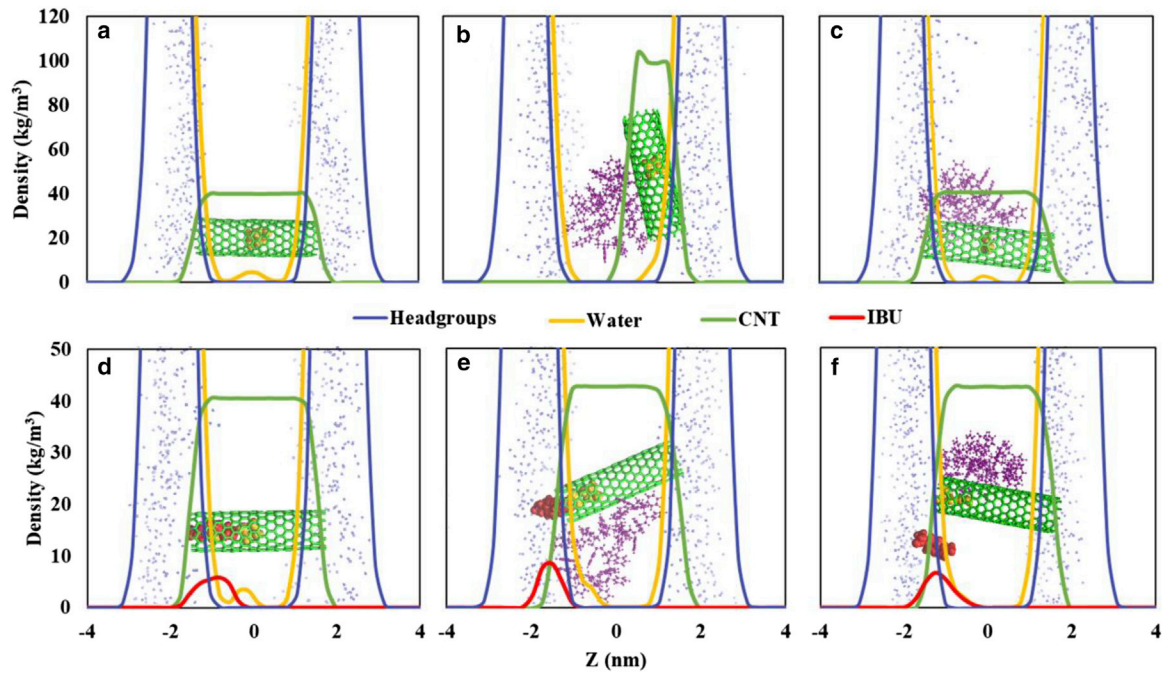
FIGURE 5 The density distributions of the lipid headgroups, water, CNT, and IBU for (*a*) POPC-CNT, (*b*) POPC-PSCNT, (*c*) POPC-carboxyl-terminated PS-functionalized CNT (PSCOOHCNT), (*d*) POPC-CNT-IBU, (*e*) POPC-PSCNT-IBU, and (*f*) POPC-PSCOOHCNT-IBU systems. The illustrations of configurations match with the lines in a color-coded manner. Polystyrene functional groups (purple) and water molecules (yellow) between lipid headgroups are not shown in the graphs to avoid confusion. To see this figure in color, go online.

molecules in the tubes results in a slightly wider tilt angle distribution range for both pristine and functionalized CNTs. Indeed, the PS-modified CNT tilts from a near-horizontal to near-vertical position in the presence of IBU. For both types of functionalized CNTs, tube internalization occurs at their nonfunctionalized ends, then the tubes rotate in the hydrophobic core of the membrane and locate in a tilted vertical configuration between upper and lower leaflets. The angle shifts reflect these configurational changes (cf. Fig. 3, *e* and *f*).

The residence time in bulk water is found to be higher with the functionalized CNTs than pristine NPs in the absence of IBU (c.f. Fig. 4 *a*). In particular, the residence time in water increases for the PSCOOH-functionalized CNT up to ~200 ns, which is attributed to the more hydrophilic nature of the NP as reported before (68). Pristine and PSCOOH-modified CNTs locate almost in the center of the bilayer, while the PS-modified CNT resides in the upper leaflet at about 1 nm distance from the bilayer core to the CNT's center of mass. When IBU is loaded into the
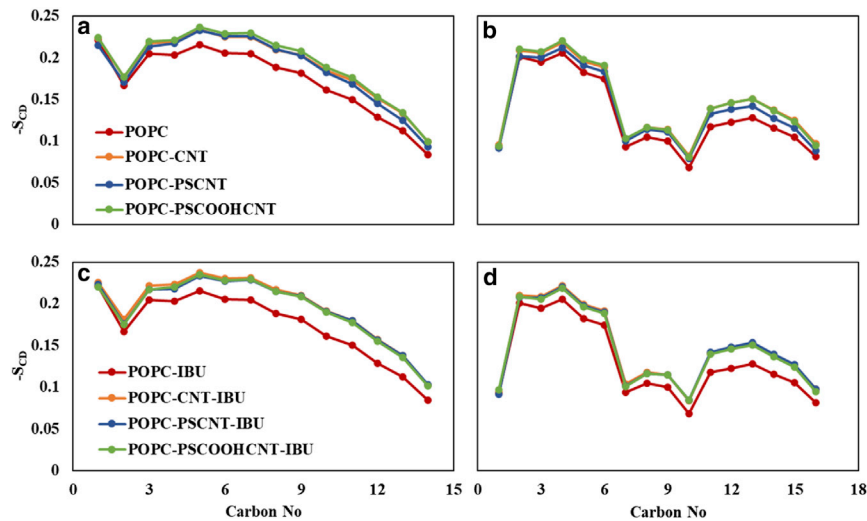

FIGURE 6 Lipid tail order parameter of sn1 (*left*) and sn2 (*right*) chains of POPC with and without IBU in the absence or presence of pristine and functionalized CNT models.

**TABLE 2 Radius of gyration (ROG) and carbon end-to-end (EtE) distances of PS functional groups attached to CNTs**

Model	Radius of gyration (nm)	End-to-end distance (nm)	
POPC-PSCNT	0.90 ± 0.02	0.89 ± 0.08	
POPC-PSCOOHCNT	0.93 ± 0.01	1.53 ± 0.14	
POPC-PSCNT-IBU	1.03 ± 0.02	2.06 ± 0.13	
POPC-PSCOOHCNT-IBU	0.91 ± 0.01	0.51 ± 0.06	

CNTs, the residence time in water shortens, and the tube insertion into the bilayer accelerates for the functionalized CNTs (c.f. Fig. 4 *b*). Especially, the PS-modified CNT penetrates the bilayer about 2.5 times faster than its unloaded counterpart. It is hypothesized that since IBU is a hydrophobic drug overall, it facilitates the uptake of functionalized CNTs by promoting hydrophobic interactions. Additionally, drug-loaded nanotubes are found to reside around the bilayer center independent of the functional groups. It should be noted that these distances are obtained from the center of mass of the CNT alone, not the center of mass of the whole NP.

To analyze the translocation of the CNTs further, density distribution profiles are obtained for CNT, IBU, and different parts of the lipid bilayer (c.f. Fig. 5). Distributions confirm the previous findings that the PS-functionalized CNT aligns perpendicular to the bilayer at 1 nm distance away from the bilayer center, while the other CNTs prefer a parallel alignment at the center of the bilayer. Furthermore, the diffusion of the CNTs facilitates the transport of water molecules across the bilayers. The open ends of the CNT allow the water molecules to penetrate inside the tube and be carried along the bilayer, as reported elsewhere (69,70). It has been argued that an open-ended nanotube may also bring about the penetration of lipid headgroups or lipid tails along the extremity of the bilayer (53). Therefore, Raczynski et al. asserted that capped nanotube gives less damage to the membrane structure and has a lower free-energy barrier to penetrate the phospholipid bilayer (71).

With the insertion of functionalized CNTs, lipid acyl tail density distributions indicate a symmetrical distortion (c.f. Figures S2 *C* and *D*). Therefore, the lipid tail order parameters are further investigated and given in Fig. 6. The presence of CNTs results in more compact and ordered lipid configurations. However, the difference in this effect is negligible between different types of CNTs, implying
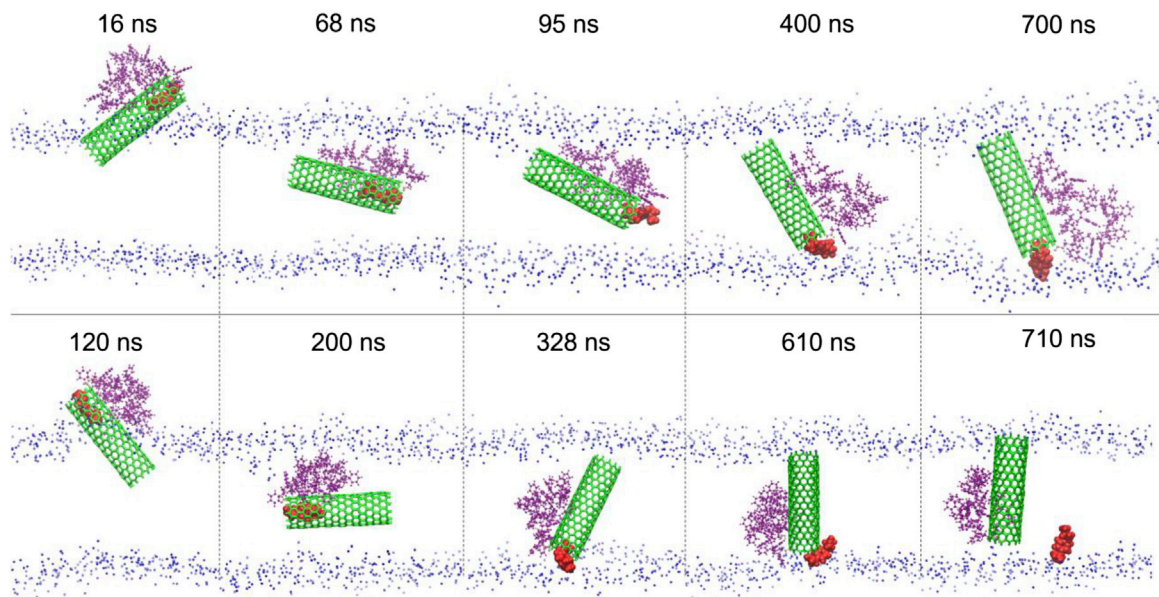
FIGURE 7 Dynamic evolution of the POPC-PSCNT-IBU system (*top panel*) and POPC-PSCOOHCNT-IBU system (*bottom panel*). Water molecules, ions, and lipid tails are not shown on the figure for clarity purposes. To see this figure in color, go online.

independence from the functionalization. That is, the lipid ordering shows a similar distribution in all CNT-containing systems.

Polymer size comparable to bilayer thickness was found to be partition into the lipid membranes, while long polymer chains form stable solid phases (72). Similarly, it was observed that low molecular weight (25 monomers) PS preferably interacts with the hydrophobic region of the bilayer than with water (73). Since, in our study, we use low molecular weight PS (29 monomers), the interactions between the functionalized CNTs and the membrane is driven by the hydrophobic interactions, and the NPs penetrating the bilayer. The PS functional groups are analyzed in terms of the radius of gyration (ROG) and carbon end-to-end (EtE) distances of the chain through the course of the simulations. Results are shown in Table 2. ROG values are between 0.9 and 1.0 nm for a 29 monomer PS chain in the absence of IBU. When IBU is present, the ROG value increases by about 15% for the PS-functionalized CNT, and the PS chain exhibits a more dispersed structure. The EtE distance also increases about 2.3-fold, since, when the IBU is stuck at the lower end of the tube, the free end of polymer spreads toward the upper end. Conversely, carboxyl modification of the PS chain provides an interactive site with the linker amide group, and the hydrophilic end of IBU strengthens this interaction before its release. Consequently, amide and carboxyl groups approach each other by reducing EtE distance to one-third.

IBU is a poorly water-soluble drug comprised of a hydrophobic tail and a hydrophilic carboxyl cap. Different chiral forms of IBU molecules have been shown to insert and remain in SWCNT in water through their methyl side chains by MD simulations (74). Therefore, here, a molecule of IBU has been placed into the center of the CNTs to investigate its delivery through the POPC bilayer. For all studied cases, IBU remains within the tubes while in water, and IBU-loaded CNTs cross the upper leaflet of the bilayer then direct the drug to the headgroups of the lower leaflet. After a 600 ns simulation time, IBU was still inside the tube in the lower end of the pristine CNT. On the other hand, at about 100 ns, the hydrophobic tail of IBU in the PS-functionalized CNT came out of the tube. Then, the hydrophilic end interacted with the lower end of the tube and positioned close to the amide group, to which the PS is attached until the end of simulation time (i.e., 700 ns). IBU in the carboxyl-terminated PS-functionalized CNT exhibits similar behavior. However, at 610 ns, the hydrophilic end of the drug also left the tube and interacted with the headgroups of the membrane. The dynamic evolution of the IBU in functionalized CNTs is demonstrated in Fig. 7. The released drug positions such that its hydrophilic end interacts with the headgroups of the membrane, while its hydrophobic tail tends toward the hydrophobic region of the membrane. It should be noted that the release of IBU is likely to be observed with hydrogen-terminated PS-functionalized CNTs in a longer timescale and can be investigated further at a coarse-grained level.

In conclusion, we developed atomistic models of PS and PSCOOH-modified SWCNTs and examined their interactions with a model lipid bilayer including/excluding the drug IBU. We demonstrate the results upon PS modification of CNTs for the first time and show that PS has a high potential to be used as a functional group for safe and enhanced drug delivery. In the future, we will expand our research by analyzing these systems at a coarse-grained level for longer times and in more realistic environments.

SUPPORTING MATERIAL

Supporting material can be found online at https://doi.org/10.1016/j.bpj.2022.10.014.

AUTHOR CONTRIBUTIONS

G.G. helped design the project, carried out simulations and simulation analysis, and wrote the article. R.F. helped design the project and supervised the simulations and simulation analysis and helped write the article. N.I.-E. designed the project and supervised the simulations and simulation analysis and helped write the article.

ACKNOWLEDGMENTS

DECLARATION OF INTERESTS

The authors declare no competing interests.

REFERENCES

1. Bianco, A., K. Kostarelos, and M. Prato. 2005. Applications of carbon nanotubes in drug delivery. *Curr. Opin. Chem. Biol.* 9:674–679.

2. Liu, Z., S. Tabakman, …, H. Dai. 2009. Carbon nanotubes in biology and medicine: in vitro and in vivo detection, imaging and drug delivery. *Nano Res.* 2:85–120.

3. De Volder, M. F. L., S. H. Tawfick, …, A. J. Hart. 2013. Carbon nanotubes: present and future commercial applications. *Science.* 339:535–539.

4. Kostarelos, K., L. Lacerda, …, A. Bianco. 2007. Cellular uptake of functionalized carbon nanotubes is independent of functional group and cell type. *Nat. Nanotechnol.* 2:108–113.

5. Jin, H., D. A. Heller, …, M. S. Strano. 2009. Size-dependent cellular uptake and expulsion of single-walled carbon nanotubes: single particle tracking and a generic uptake model for nanoparticles. *ACS Nano.* 3:149–158.

6. Lamprecht, C., B. Plochberger, …, A. Ebner. 2014. A single-molecule approach to explore binding, uptake and transport of cancer cell targeting nanotubes. *Nanotechnology.* 25:125704.

7. Yan, H., Z. Xue, …, J. Li. 2019. Toxicity of carbon nanotubes as anti-tumor drug carriers. *Int. J. Nanomedicine.* 14:10179–10194.

8. Huang, W., S. Fernando, …, Y. P. Sun. 2003. Solubilization of single-walled carbon nanotubes with diamine-terminated oligomeric poly(-ethylene glycol) in different functionalization reactions. *Nano Lett.* 3:565–568.

9. Naqvi, S. T. R., T. Rasheed, …, R. Nawaz. 2020. Modification strategies for improving the solubility/dispersion of carbon nanotubes. *J. Mol. Liq.* 297:111919.

10. Ma, P. C., N. A. Siddiqui, …, J. K. Kim. 2010. Dispersion and functionalization of carbon nanotubes for polymer-based nanocomposites: a review. *Compos. Appl. Sci. Manuf.* 41:1345–1367.

11. Nish, A., J. Y. Hwang, …, R. J. Nicholas. 2007. Highly selective dispersion of single-walled carbon nanotubes using aromatic polymers. *Nat. Nanotechnol.* 2:640–646.

12. Dumortier, H., S. Lacotte, …, A. Bianco. 2006. Erratum: functionalized carbon nanotubes are non-cytotoxic and preserve the functionality of primary immune cells (Nano Letters (2006) 6 (1527. *Nano Lett.* 6:3003.

13. Liu, Z., W. Cai, …, H. Dai. 2007. In vivo biodistribution and highly efficient tumour targeting of carbon nanotubes in mice. *Nat. Nanotechnol.* 2:47–52.

14. Kostarelos, K. 2008. The long and short of carbon nanotube toxicity. *Nat. Biotechnol.* 26:774–776.

15. Bhirde, A. A., S. Patel, …, J. F. Rusling. 2010. Distribution and clearance of PEG-single-walled carbon nanotube cancer drug delivery vehicles in mice. *Nanomedicine.* 5:1535–1546.

16. Liu, Z., C. Davis, …, H. Dai. 2008. Circulation and long-term fate of functionalized, biocompatible single-walled carbon nanotubes in mice probed by Raman spectroscopy. *Proc. Natl. Acad. Sci. USA.* 105:1410–1415.

17. Prencipe, G., S. M. Tabakman, …, H. Dai. 2009. PEG branched polymer for functionalization of nanomaterials with ultralong blood circulation. *J. Am. Chem. Soc.* 131:4783–4787.

18. Schipper, M. L., N. Nakayama-Ratchford, …, S. S. Gambhir. 2008. A pilot toxicology study of single-walled carbon nanotubes in a small sample of mice. *Nat. Nanotechnol.* 3:216–221.

19. Krajcik, R., A. Jung, …, O. Zolk. 2008. Functionalization of carbon nanotubes enables non-covalent binding and intracellular delivery of small interfering RNA for efficient knock-down of genes. *Biochem. Biophys. Res. Commun.* 369:595–602.

20. Bobadilla, A. D., E. L. G. Samuel, …, J. M. Seminario. 2013. Calculating the hydrodynamic volume of poly(ethylene oxylated) single-walled carbon nanotubes and hydrophilic carbon clusters. *J. Phys. Chem. B.* 117:343–354.

21. Lee, H. 2013. Molecular dynamics studies of pegylated single-walled carbon nanotubes: the effect of PEG size and grafting density. *J. Phys. Chem. C.* 117:26334–26341.

22. Gul, G., R. Yildirim, and N. Ileri-Ercan. 2021. Cytotoxicity analysis of nanoparticles by association rule mining. *Environ. Sci, Nano.* 8:937–949.

23. Qian, D., E. C. Dickey, …, T. Rantell. 2000. Load transfer and deformation mechanisms in carbon nanotube-polystyrene composites. *Appl. Phys. Lett.* 76:2868–2870.

24. Chadwick, R. C., U. Khan, …, A. Adronov. 2013. Polymer grafting to single-walled carbon nanotubes: effect of chain length on solubility, graft density and mechanical properties of macroscopic structures. *Small.* 9:552–560.

25. Hill, D. E., Y. Lin, …, Y.-P. Sun. 2002. Functionalization of carbon nanotubes with polystyrene. *Macromolecules.* 35:9466–9471.

26. Huang, H. M., I. C. Liu, …, R. C. C. Tsiang. 2004. Preparing a polystyrene-functionalized multiple-walled carbon nanotubes via covalently linking acyl chloride functionalities with living polystyryllithium. *J. Polym. Sci. A. Polym. Chem.* 42:5802–5810.

27. Li, H., F. Cheng, …, A. Adronov. 2005. Functionalization of single-walled carbon nanotubes with well-defined polystyrene by "click" coupling. *J. Am. Chem. Soc.* 127:14518–14524.

28. Tabet, L., C. Bussy, …, S. Lanone. 2011. Coating carbon nanotubes with a polystyrene-based polymer protects against pulmonary toxicity. *Part. Fibre Toxicol.* 8:3–13.

29. Li, Y., W. Xu, …, L. Gao. 2015. Folate functionalized carbon nanotubes for delivery and controlled release of ibuprofen. *J. Funct. Mater.* 46:13070–13073.

30. Rostamizadeh, K., M. Habibizadeh, …, A. Ramazani. 2017. Preparation and characterization of PEGylated multiwall carbon nanotubes as covalently conjugated and non-covalent drug carrier: a comparative study. *Mater. Sci. Eng. C Mater. Biol. Appl.* 74:1–9.

31. Choi, Y. K., N. R. Kern, …, W. Im. 2022. CHARMM-GUI nanomaterial modeler for modeling and simulation of nanomaterial systems. *J. Chem. Theor. Comput.* 18:479–493.

32. Choi, Y. K., S. J. Park, …, W. Im. 2021. CHARMM-GUI polymer builder for modeling and simulation of synthetic polymers. *J. Chem. Theor. Comput.* 17:2431–2443.

33. Kim, S., J. Lee, …, W. Im. 2017. CHARMM-GUI ligand reader and modeler for CHARMM force field generation of small molecules. *J. Comput. Chem.* 38:1879–1886.

34. Jo, S., T. Kim, and W. Im. 2007. Automated builder and database of protein/membrane complexes for molecular dynamics simulations. *PLoS One.* 2:e880.

35. Wu, E. L., X. Cheng, …, W. Im. 2014. CHARMM-GUI membrane builder toward realistic biological membrane simulations. *J. Comput. Chem.* 35:1997–2004.

36. Lee, J., X. Cheng, …, W. Im. 2016. CHARMM-GUI input generator for NAMD, GROMACS, AMBER, OpenMM, and CHARMM/OpenMM simulations using the CHARMM36 additive force field. *J. Chem. Theor. Comput.* 12:405–413.

37. Jo, S., T. Kim, …, W. Im. 2008. CHARMM-GUI: a web-based graphical user interface for CHARMM. *J. Comput. Chem.* 29:1859–1865.

38. Berendsen, H. J. C., D. van der Spoel, and R. van Drunen. 1995. GROMACS: a message-passing parallel molecular dynamics implementation. *Comput. Phys. Commun.* 91:43–56.

39. Humphrey, W., A. Dalke, and K. Schulten. 1996. VMD: visual molecular dynamics. *J. Mol. Graph.* 14:33–38.

40. Riggs, J. E., Z. Guo, …, R. V December. 2000. Strong luminescence of solubilized carbon nanotubes. *J. Am. Chem. Soc.* 122:5879–5880.

41. Czerw, R., Z. Guo, …, D. L. Carroll. 2001. Organization of polymers onto carbon nanotubes: a route to nanoscale Assembly. *Nano Lett.* 1:423–427.

42. Huang, W., Y. Lin, …, Y. P. Sun. 2002. Sonication-assisted functionalization and solubilization of carbon nanotubes. *Nano Lett.* 2:231–234.

43. Yang, Y., X. Xie, …, Y.-W. Mai. 2006. Synthesis and self-assembly of polystyrene-grafted multiwalled carbon nanotubes with a hairy-rod nanostructure. *J. Polym. Sci. A. Polym. Chem.* 44:3869–3881.

44. Huang, J., and A. D. Mackerell. 2013. CHARMM36 all-atom additive protein force field: validation based on comparison to NMR data. *J. Comput. Chem.* 34:2135–2145.

45. Huang, J., S. Rauscher, …, A. D. MacKerell, Jr. 2017. CHARMM36m: an improved force field for folded and intrinsically disordered proteins. *Nat. Methods.* 14:71–73.

46. Klauda, J. B., R. M. Venable, …, R. W. Pastor. 2010. Update of the CHARMM all-atom additive force field for lipids: validation on six lipid types. *J. Phys. Chem. B.* 114:7830–7843.

47. Venable, R. M., A. J. Sodt, …, J. B. Klauda. 2014. CHARMM all-atom additive force field for sphingomyelin: elucidation of hydrogen bonding and of positive curvature. *Biophys. J.* 107:134–145.

48. Vanommeslaeghe, K., E. Hatcher, …, A. D. MacKerell, Jr. 2010. CHARMM General Force Field (CGenFF): a force field for drug-like molecules compatible with the CHARMM all-atom additive biological force fields. *J. Comput. Chem.* 31:671–690.

49. Pramanik, C., J. R. Gissinger, …, H. Heinz. 2017. Carbon nanotube dispersion in solvents and polymer solutions: mechanisms, assembly, and preferences. *ACS Nano.* 11:12805–12816.

50. Ham, H. T., C. M. Koo, …, I. J. Chung. 2004. Chemical modification of carbon nanotubes and preparation of polystyrene/carbon nanotubes composites. *Macromol. Res.* 12:384–390.

51. Liu, Y. H., G. Wang, …, W. H. Wang. 2007. Preparation and characterization of polystyrene modified single-walled carbon nanotube. *Science.* 315:1385–1388.

52. Mountrichas, G., S. Pispas, and N. Tagmatarchis. 2008. Grafting-to approach for the functionalization of carbon nanotubes with polystyrene. *Mater. Sci. Eng., B.* 152:40–43.

53. Kraszewski, S., A. Bianco, …, C. Ramseyer. 2012. Insertion of short amino-functionalized single-walled carbon nanotubes into phospholipid bilayer occurs by passive diffusion. *PLoS One.* 7:e40703–e40711.

54. Bussi, G., D. Donadio, and M. Parrinello. 2007. Canonical sampling through velocity rescaling. *J. Chem. Phys.* 126:014101.

55. Darden, T., D. York, and L. Pedersen. 1993. Particle mesh Ewald: an N·log(N) method for Ewald sums in large systems. *J. Chem. Phys.* 98:10089–10092.

56. Parrinello, M., and A. Rahman. 1981. Polymorphic transitions in single crystals: a new molecular dynamics method. *J. Appl. Phys.* 52:7182–7190.

57. Kučerka, N., S. Tristram-Nagle, and J. F. Nagle. 2005. Structure of fully hydrated fluid phase lipid bilayers with monounsaturated chains. *J. Membr. Biol.* 208:193–202.

58. Kučerka, N., M. P. Nieh, and J. Katsaras. 2011. Fluid phase lipid areas and bilayer thicknesses of commonly used phosphatidylcholines as a function of temperature. *Biochim. Biophys. Acta Biomembr.* 1808:2761–2771.

59. Kraszewski, S., F. Picaud, …, C. Ramseyer. 2012. How long a functionalized carbon nanotube can passively penetrate a lipid membrane. *Carbon N. Y.* 50:5301–5308.

60. Gao, Y., D. Mao, …, S. Zeng. 2019. Carbon nanotubes translocation through a lipid membrane and transporting small hydrophobic and hydrophilic molecules. *Appl. Sci.* 9:4271.

61. Raffa, V., G. Ciofani, …, A. Cuschieri. 2008. Can the properties of carbon nanotubes influence their internalization by living cells? *Carbon N. Y.* 46:1600–1610.

62. Geng, J., K. Kim, …, A. Noy. 2014. Stochastic transport through carbon nanotubes in lipid bilayers and live cell membranes. *Nature.* 514:612–615.

63. Tran, I. C., R. H. Tunuguntla, …, T. Van Buuren. 2016. Structure of carbon nanotube porins in lipid bilayers: an in situ small-angle X-ray scattering (SAXS) study. *Nano Lett.* 16:4019–4024.

64. Sullivan, K., Y. Zhang, …, A. Noy. 2020. Carbon nanotube porin diffusion in mixed composition supported lipid bilayers. *Sci. Rep.* 10:11908.

65. Höfinger, S., M. Melle-Franco, …, F. Zerbetto. 2011. A computational analysis of the insertion of carbon nanotubes into cellular membranes. *Biomaterials.* 32:7079–7085.

66. Lopez, C. F., S. O. Nielsen, …, M. L. Klein. 2004. Understanding nature's design for a nanosyringe. *Proc. Natl. Acad. Sci. USA.* 101:4431–4434.

67. Vögele, M., J. Köfinger, and G. Hummer. 2018. Molecular dynamics simulations of carbon nanotube porins in lipid bilayers. *Faraday Discuss.* 209:341–358.

68. Gul, G., and N. Ileri-Ercan. 2021. Fullerene translocation through peroxidized lipid membranes. *RSC Adv.* 11:7575–7586.

69. Lopez, C. F., S. O. Nielsen, …, M. L. Klein. 2005. Structure and dynamics of model pore insertion into a membrane. *Biophys. J.* 88:3083–3094.

70. Wallace, E. J., and M. S. P. Sansom. 2008. Blocking of carbon nanotube based nanoinjectors by lipids: a simulation study. *Nano Lett.* 8:2751–2756.

71. Raczyński, P., K. Górny, …, Z. Gburski. 2013. Nanoindentation of biomembrane by carbon nanotubes - MD simulation. *Comput. Mater. Sci.* 70:13–18.

72. Bochicchio, D., L. Cantu, …, E. Del Favero. 2022. Polystyrene perturbs the structure, dynamics, and mechanical properties of DPPC membranes: an experimental and computational study. *J. Colloid Interface Sci.* 605:110–119.

73. Rossi, G., J. Barnoud, and L. Monticelli. 2014. Polystyrene nanoparticles perturb lipid membranes. *J. Phys. Chem. Lett.* 5:241–246.

74. Farhadian, N. 2013. Investigating the ibuprofen chiral forms interactions with single wall carbon nanotube. *Int. J. Nanosci. Nanotechnol.* 9:127–138.